Polarimetric signatures of sea ice
Part I: Theoretical model

S. V. Nghiem, R. Kwok,
S. H. Yueh, and M. R. Drinkwater
Jet Propulsion Laboratory
California Institute of Technology
Pasadena, California

Mail: JPL, MS 300-235, 4800 Oak Grove Dr., Pasadena, CA 91109

Polarimetric signatures of sea ice
Part I: Theoretical model

S. V. Nghiem, R. Kwok, S. H. Yueh, and M. R. Drinkwater

Jet Propulsion Laboratory, California Institute of Technology, Pasadena, California

Physical, structural, and electromagnetic properties and interrelating processes in sea ice are used to develop a composite model for polarimetric backscattering signatures of sea ice. Physical properties of sea ice constituents such as ice, brine, air, and salt are presented in terms of their effects on electromagnetic wave interactions. Sea ice structure and geometry of scatterers are related to wave propagation, attenuation, and scat tering. Temperature and salinity, which are determining factors for the thermodynamic phase distribution in sea ice, are consistently used to derive both effective permittivities and polarimetric scattering coefficients, Polarimetric signatures of sea ice depend on crystal sizes and brine volumes, which are affected by ice growth rates, Desalination by brine expulsion, drainage, or other mechanisms modifies wave penetration and scattering. Sea ice signatures are further complicated by surface conditions such as rough interfaces, hummocks, snow cover, brine skim, slush layer, Based on the same set of geophysical parameters characterizing sea ice, a composite model is developed to calculate effective permittivities and backscattering covariance matrices at microwave frequencies for interpretation of sea ice polarimetric signatures.

1. INTRODUCTION

Sea ice is important to global climate because of its role in the mass balance and heat transfer processes bet ween the ocean and the atmosphere [*Maykut, 1978; 1982; Wettlaufer,* 1994. Global monitoring of sea ice with polarimetric remote sensing has drawn considerable interests [*Rignot and Drinkwater, 1994;" Cavalieri et al., 1991*]. To interpret sea ice signatures in polarimetric remote sensing data, it is necessary to relate electromagnetic scattering effects of sea ice to its physical and structural properties. This relationship provides insight into sea ice properties that influence electromagnetic scattering mechanisms and determine polarimetric signatures of sea ice,

Here, the purpose is to relate sea ice characteristics and processes to active polarimetric signatures of sea ice through the development of a model based on sea ice properties. This is presented in a series of two papers: (1) Part I: Theoretical model and (2) Part II: Experimental observations. In this first paper of the series, sea ice properties are discussed and then used to develop a composite model for understanding polarimetric signatures of sea ice including volume and surface scattering mechanisms at microwave frequencies. Voluminous polarimetric measurements of various sea ice types in the Beaufort sea have been archived in the library of data acquired by the Jet Propulsion Laboratory multi-frequency polarimetric Synthetic Aperture Radar, Expeditions and experiments for sea ice characterizations spanning over several decades have collected numerous physical parameters of sea ice. The composite model in this paper provides a link between the observed polarimetric signatures to the measured sea ice properties. In part II, the model will be used to explain experimental observations of sea ice.

Sea ice has long been a subject of intensive research. Extensive results from studies of sea *ice* and its major constituent, ice, have been reported in classical publications such as Ice *Physics [Hobbs, 1974], The Physics of Ice [Glen, 1974],* and *The Growth, Structure, and Properties of Sea Ice [Weeks and Ackley, 1982],* The complexity of sea ice is attributed to its inhomogeneous composition, tryst allograph, st ructure, growth process, thermodynamic

variations, and environmental effects, Interactions among the physical processes in sea ice result in the intricate relationship among physical, structural, and electromagnetic properties of sea ice.

To a limited extent, sea ice properties have been used in calculations of conventional backscattering coefficients [Lee *and Kong, 1985; Tjuatja et al, 1992*] and fully polarimetric scattering coefficients [*Borgeaud et al., 1989; Nghiem et al., 1990*]. However, one or more of the following have been assumed: independence of interrelated sea ice parameters, effective isotropy in the sea ice medium, spherical scatterers or aligned spheroids, uniform thickness, flat interfaces, no snow or slush or brine layer, and multi-year ice without hummocks. These assumptions, however, simplify certain properties of sea ice and thus limit the understanding of sea ice signatures.

Affected by inhomogeneities in sea ice, wave propagation, attenuation, and polarimetric scattering, are interrelated and linked to physical and structural properties of sea ice. The isotropy assumption contradicts the preferential vertical structure in columnar sea ice, which constitutes a significant fraction in the global sea ice mass. Spherical scatterers and untilted aligned spheroids cannot account for depolarization effects in sea ice polarimetric signatures in first-order scattering. Furthermore, shapes of scatterers and their orientations influence wave interactions in sca ice even in zeroth-order effects.

A uniform thickness of an optically thin ice sheet causes oscillations in sea ice signatures while a distribution in thickness weakens or even erases these oscillations. Volume inhomogeneities in sea ice with flat interfaces give low backscattering from sea ice at small incident angles. Rough interfaces without volume inhomogeneities underestimate scattering magnitudes, depolarization, and decorrelation effects at large incident angles. Snow, slush, brine covers, and hummocks modify sea ice scattering and need to be considered to interpret sea ice polarimetric signatures.

In the following sections, sea ice physical, structural, electromagnetic properties, and their interrelations and variations imposed by the physical processes of sea ice growth,

desalination, and environmental effects are presented. The complexity of these sea ice properties is encompassed in the composite model, The model includes the thermodynamic phase distribution of sea ice constituents, wave speed modification and scattering loss in inhomogeneous media, and ellipsoidal inclusions for polarimetric volume scattering. Effective anisotropy of sea ice due to the preferential vertical alignment of brine inclusions and random azimuthal orientations of crystallographic c-axes in sea ice is considered. Thickness distribution in a sea ice layer, snow cover with randomly oriented spheroidal ice grains, brine skim and slush layer with high salinity, multiple wave interactions with boundaries in anisotropic layered media are modeled. Rough surfaces at layer interfaces with wave attenuation and differential phase delay through the layered media and effects of hummock topography on both volume and surface scattering mechanisms are accounted for. Physical meanings conveyed in mathematical expressions for sea ice signatures are explained. Polarimetric data interpretations with the composite model for experimental observations of sea ice in the Beaufort sea will be presented in the second paper.

2. CHARACTERISTICS OF SEA ICE

A background of sea ice characteristics is necessary to consider the realistic complexity of sea ice in the modeling and to define domains of model input parameters constrained by the sea ice physics. This section presents sea ice characteristics in the context of their interrelationship with electromagnetic properties for the development of a polarimetric composite model of sea ice.

2.1. Sea Ice Constituents

Sea ice is an inhomogeneous medium composed of an ice background, brine inclusions, air bubbles, and solid salt. Electromagnetic properties of these constituents are characterized by permeabilities and permittivities, which relate material characteristics to

electromagnetic fields by constitutive relations [Kong, 1986]. The sea ice constituents arc non-magnetic materials and their permeability is μ_0 (4π x 10^{-7} H/m), Air has a real permittivity of ϵ_0 (8.8542 x 10^{-12} F/m). However, permittivities of other sea icc constituents are complex quantities, with real parts for wave speeds and imaginary parts for wave at tenuat ions.

Icc is a dispersive medium whose complex permittivity changes with electromagnetic wave frequency. The imaginary part of ice permittivity varies by two orders of magnitude as a function of frequency [Evans, 1965]. For sea-water brine, the absolute value of the permittivity is more than one order of magnitude larger than that of ice in the microwave frequency range: Both real and imaginary parts of brine permittivity decrease by several times as frequency increases [*Stogryn and Desargant, 1985*]. Although solid salt volume is usually minute compared to the other constituents, the precipitation process of salt at the eutectic temperature redistributes the phase of brine and air inclusions. Mixing of these constituents with different phases determines the effective permittivity of sca ice.

With permittivity contrasts to the ice background, inhomogeneities act as scattering sources induced by an incident electromagnetic field, giving rise to the source terms in inhomogeneous vector wave equations. These current sources radiate electromagnetic fields in all directions into the upper medium, where the scattered waves arc measured at all linear polarization combinations. The inhomogeneities in sea ice are responsible for effective wave propagation, attenuation, and scattering which are interrelated and linked to the properties of the constituents in sea ice.

2.2. *Crystallography and Structure*

In natural geophysical conditions, the ordinary ice polymorph (ice I_h) is predominant *[Hobbs, 1974; Glen, 1974; Weeks and Ackley, 1982]*. Other crystallographic phases of ice are formed at very low temperatures or high pressures. As illustrated in Figure 1, ice I_h has a hexagonal symmetry with oxygen atoms packed closely in parallel planes called

basal planes [*Petrenko*, 1993]. The crystallographic c-axis (principal hexagonal axis) is perpendicular to the basal planes and the a-axes arc parallel to these planes, Natural ice is a polycrystalline medium composed of many single crystals with different orientations. Beneath a thin transition layer, sea ice becomes columnar in structure with c-axes parallel to within a few degrees of the horizontal plane [*Weeks and Ackley,1982*].

A polycrystal in sea ice consists of small parallel ice plates referred as ice platelets. Sca water is trapped in pockets between these ice platelets, depicted in Figure 2, during the growth of sea ice, As the ice grows and the temperature decreases, fresh water in the pockets freezes to the platelet walls, leaving liquid in the pockets more saline. These brine inclusions have a high permittivity that strongly affects electromagnetic properties of sea ice. Horizontal thin sections and vertical micrographs of sea ice reveal a substantially ellipsoidal shape of brine inclusions [*Weeks* and *Ackley,1982; Arcone et al., 1986]*. Because the c-axes arc parallel to the horizontal plane, the ice platelets are vertical, Consequently, ellipsoidal brine inclusions, sandwiched between the platelets, are preferentially oriented in the vertical direction. Unless c-axes are aligned by an underlying sea current [*Weeks* and Gow, 1978], the inclusions have random azimuthal orientations in the horizontal plane as shown in Figure 3.

This orientation distribution of brine inclusions in the ordinary ice polymorph renders the effective permittivity of sea ice uniaxially anisotropic with the optic axis in the vertical direction [*Nghiem et al.,1993 b*]. The vertical anisotropy in sea ice effectively supports two characteristic **waves,** ordinary and extraordinary [*Kong*, 1986], propagating at different speeds and attenuation rates. First-year sea ice, especially young ice, contains many brine inclusions and their properties are carried in sea ice polarimetric signatures. In multi-year sea ice, because of the desalination in the growth process (Section 2.4), the inhomogeneities arc predominantly air bubbles, which are more rounded and thus multi-year sea ice becomes more isotropic [*Nghiem et al., 1993c*].

2.3. Temperature and Salinity

Temperature and salinity arc two of the most important characterization parameters of sea ice, Under stable condition, temperature in a sea ice layer distributed linearly from the top interface with cold air to the bottom interface with warmer sca water. Many measurements of sea ice temperatures show "an approximately linear profile in ice depth [*Cox and Weeks, 1974; Wen et al., 1989; Gow et al., 1990; Eicken, 1992*]. In first-year sca ice, C-shape salinity distribution in ice depth is usually observed [*Wen et a/., 1989; Gow et al., 1990; Eicken, 1992*]. Upward brine expulsion and flooding are important mechanisms causing the high top salinity [*Eicken, 1992*], The high bottom salinity is obvious because of the interface between ice and saline sea water.

Electromagnetic properties of sea ice are strongly related to the temperature and salinity. These two parameters together with sea ice density govern the thermodynamic phase distribution of sea ice constituents. Fractional volumes of brine and air inclusions arc obtained from equations based on phase diagrams [*Cox and Weeks, 1983*]. Near the top of the ice layer, the temperature is low and the salinity is high (C-shape salinity profile), Deeper into the middle of the ice layer, the temperature increases while the salinity decreases. Except near the sea water interface where the brine volume is large, the distributions of temperature and salinity effectuate an approximately uniform distribution of brine volume in the ice layer [*Wen et al., 1989*]. Typically, the average brine volume of first-year sea ice in the Beaufort sea is on the order of few percent [*Wen et al., 1989; Weeks and Ackley, 1982*].

Furthermore, temperature affects permittivities of individual constituents of sea ice. Ice permittivity varies with temperature [*Tiuri et al., 1984; Mätzler and Wegmüller, 1987*]. Brine permittivity is a strong function of temperature [*Stogryn and Desargant, 1985*] and sea water permittivity depends on both temperature and salinity [*Klein and Swift, 1977*]. Temperature also affects sea ice effective permittivity by the process of salt expulsion. At the eutectic temperature of –21.2° C, a sharp phase change occurs due to the precipitation

of sodium chloride dihydrate [*Weeks and Ackley, 1982*]. Below this temperature, brine solidifies and consequently sea ice permittivity drops [*Arcone at al.,* 1986].

.2.4. *Growth and Desalination*

Ice grows dendritically at large supercooling due to the rapid growth in directions parallel to a-axes [Glen, 1974]. Columnar ice grows in the form of vertical ice platelets which preferentially align brine inclusions in the vertical direction as discussed above. Sea ice growth rate is determined by environmental conditions such as air-sea temperature difference, winds and sea currents, and heat fluxes including latent and radiative heat.

Thorndike et al. [1975] have estimated sea ice growth rate in polar oceans throughout the year. Figure 4a shows the growth rate $f(h)$ (cm/day) as a function of sea ice thickness (m) on March 11 (winter time) with the fitted function $f(h) = 12.71 - 0.2116h$ ($h \leq$ 50 cm), $2.13\exp(-0.017h)$ ($50 < h \leq 150$ cm), $0.52 - 8,67 \ x \ 10^{-4}h$ ($150 < h \leq 600$cm). From $dh/dt = 12.71 - 0.2116h$ (for ice thinner than 50 cm), the ice thickness is $h(t) = 60[1 - \exp(-0.2116t)]$ where t is the elapsed time from the initial ice growth. Thus for thin ice (O- 10 cm), the ice growth is approximately linear under the first-order expansion of $h(t)$. Figure 4b compares this growth of sea ice with NaCl ice grown under a cold plate [*Lofgren and Weeks, 1969*] and saline grown in a cold room during CRRELEX'93 (Cold Regions Research and Engineering Laboratory Experiment, September 1993). For faster growth rates, ice platelet spacing becomes narrower and the bulk salinity due to brine entrapment is higher [*Meese,* 1989, *Nakawo and Sinha, 1981; Lofgren and Weeks, 1969*]. This is a determining factor in ice crystal sizes and brine volumes.

As the ice becomes thicker, ice growth slows significantly and desalination takes place. There are several desalination mechanisms: brine migration caused by thermal gradient, expulsion by pressure in brine pockets, drainage by gravity, and flushing by surface melt water [*Meese,* 1989], It is found that the average salinity in Arctic sea ice is a piecewise linear decreasing function of ice thickness [Cox *and Weeks, 1974];* the pronounced

change in the slope of the linear salinity function of thickness corresponds to the change in the dominant desalination mechanism from brine expulsion to gravity drainage [*Cox and Weeks, 1974*] The desalination reduces the lossy brine volume and increases the air volume. As a result, the attenuation is decreased and electromagnetic waves can penetrate deeper into the ice. The waves encounter more scatterers with weaker local scattering effects since the permittivity contrast of air to ice is less than that between brine and ice. This competing effect in the scattering from sea ice needs to be accounted for in the model to interpret the scattering signature of multi-year sea ice, which experiences significant desalination.

2.5. Surface Effects: Roughness, Snow, Slush, and Brine Covers

Physical properties of sea ice are further complicated by surface effects such as roughness, snow, slush, and brine covers. Undeformed first- year sea ice is usually smooth with some small scale roughness. Roughness contributes to the total backscattering especially at small incident angles. Moreover, multi-year ice undergoes differential melt which results in hummock. with meter-scale lengths, From hummock profiles of air-snow and snow-ice interfaces of multi-year ice in the Beaufort sea (Figure 5a) [*Cox and Weeks, 1974*], large-scale correlation functions are obtained and shown in Figures 5b and 5c. The hummock topography tilts local sea ice surface areas and modulates the small scale roughness. Thus, the large scale hummocks modify both the volume and surface scattering properties of sea ice.

Snow cover on sea ice introduces an additional scattering layer and also causes physical changes in sea ice. While the sea ice layer is anisotropic, the snow medium is effectively isotropic because of random orientations of ice grains in snow [*Sihvola et al., 1988; Nghiem et al., 1993 b*]. The isotropic snow cover has a masking effect which lessens the anisotropic characteristics in the polarimetric signature of columnar sea ice. Furthermore, snow capillary force gives rise to brine wicking, especially for thin ice [*Drinkwater and Crocker*, 1988].

Consequently, a slush layer with high salinity appears between the snow and the ice layer. This slush layer has a high permittivity that strongly influences the scattering from sea ice. A highly saline surface skim, or a thin brine layer, has been observed on the surface of young lead ice [*Richter-Menge and Perovich, 1992; Drinkwater and Crocker, 1988*]. The brine layer significantly impacts polarimetric signatures of sea ice.

3. POLARIMETRIC COMPOSITE MODELS

Based on the properties of sea ice discussed above, a composite model for polarimetric signatures of sea ice is developed and presented here. Both effective permittivities and polarimetric scattering coefficients are derived from the same set of sea ice properties. Their interrelationship is therefore accounted for and linked to sea ice physical and structural properties and processes.

Sea ice covered by a layer of snow, slush, or brine is modeled with a layered configuration as illustrated in Figure 6. The upper half space is air with permittivity ϵ_0 and permeability μ_0. Region 1 is described as an isotropic inhomogeneous medium containing randomly oriented spheroidal scatterers with a spatially dependent permittivity $\epsilon_1(\bar{r})$. Sea ice in Region 2 is an inhomogeneous medium, with permittivity $\epsilon_2(\bar{r})$, composed of an ice background with ellipsoidal brine inclusions whose orientation renders the medium effectively anisotropic. For multi-year ice, air bubbles are included in the ice layer. Region 3 is the homogeneous sea water with permittivity ϵ_3. Amplitude vectors described in Figure 7 for up and downgoing waves will be used to derive multiple wave interactions with boundaries in the layered media.

Effective permittivities of inhomogeneous media are obtained with the strong permittivity fluctuation theory. Covariance matrices, whose elements are polarimetric scattering coefficients characterizing polarimetric signatures of sea ice, are then calculated with the analytic wave theory which preserves the phase information. Small scale roughnesses and

large scale hummock topography are also considered. Wave scattering mechanisms in the inhomogeneous anisotropic layered media with composite interfaces are illustrated in Figure 8 and modeled in the following sections to derive polarimetric signatures of sea ice,

3.1 Effective Permittivities of Inhomogeneous Media

The mixing of the constituents in the inhomogeneous sea ice determines an effective permittivity which governs wave propagation and attenuation in the medium. In this model, the dispersion of sea ice not only depends on the dispersive permittivity of each constituent but also on the scattering effect of the inhomogeneities in addition to the quasi-static part. Effective permittivities of sea ice are derived from the strong permittivity fluctuation theory [*Tsang and Kong, 1981*] which is extended to account for randomly oriented spheroidal scatterers [*Yueh et al., 1990; Nghiem et al., 1999a]*, and for ellipsoidal scatterers [*Nghiem et al., 1993b*]. Results for effective permit ttivities are summarized here and their physical meanings are pointed out in terms of sea ice properties.

Consider medium n, with $n = 1$ for the cover layer such as snow and $n = 2$ for the sea ice layer (see Figure 6). Generally to account for the medium anisotropy, the effective permittivity is described by the tensor

$$\bar{\bar{\epsilon}}_{neff} = \bar{\bar{\epsilon}}_{ng} + \epsilon_0 \left[\bar{\bar{I}} - \bar{\bar{\xi}}_{neff} \cdot \langle \bar{\bar{S}}_n \rangle \right]^{-1} \cdot \bar{\bar{\xi}}_{neff} \tag{1}$$

where $\bar{\bar{I}}$ is the unit dyad, $\bar{\bar{\epsilon}}_{ng}$ is the auxiliary permittivity, $\bar{\bar{S}}_n$ is the dyadic coefficient, and $\bar{\bar{\xi}}_{neff}$ is the effective dyadic scatterer [*Tsang and Kong, 1981*].

Mathematically, the first term, $\bar{\bar{\epsilon}}_{ng}$, in (1) together with the dyadic coefficient $\bar{\bar{S}}_n$ are determined by the condition of secular-term elimination, The secular term originates from the singularity corresponding to the coincidence of an observation point and a source point in the inhomogeneous medium, The results for $\bar{\bar{\epsilon}}_{ng}$ can be reduced to a generalized form of the Polder - van Santen dielectric mixing formula [*Tsang and Kong, 1985*].

Physically, $\bar{\bar{\epsilon}}_{ng}$ is the effective permittivity under the quasi-static condition. It characterizes wave propagation in an effective medium without the scattering effects, From

the functional forms of $\bar{\bar{\epsilon}}_{ng}$ [*Nghiem et al., 1993a, 1993b*], it is observed that

$$\bar{\bar{\epsilon}}_{ng} = \bar{\bar{\epsilon}}_{ng}(f_{nc}, \epsilon_{nc}\cdot\epsilon_{ng}, \; [\bar{\bar{S}}_n]) \qquad (2)$$

where subscript c denotes a constituent in the inhomogeneous media, As indicated in (2), $\bar{\bar{\epsilon}}_{ng}$ is a function of fractional volume f_{nc} of the medium constituents, permittivity contrast $(\epsilon_{nc}\text{-}\epsilon_{ng})$, and dyadic coefficient clement $[\bar{\bar{S}}_n]$.

In sea ice $(n = 2)$, the constituents are ice $(c = ice)$, brine $(c = brine)$, or air $(c = air)$ as discussed in Section 2.1. The fractional volumes of these constituents follow the thermodynamic phase distribution determined by the temperature, salinity, and density of sea ice (Section 2.3), Constituent Permittivities are complex and vary with frequency, temperature, and salinity (Sections *2.1* and *2.3)*. In first-year sea ice, brine inclusions and the ice background have a large permittivity contrast (Section 2.1) which strongly affects wave propagation and attenuation in sea ice. In desalinated multi-year sea ice (Section 2.4,), the permittivity contrast between air bubbles and ice is smaller, wave speed is larger, absorption, and wave penetration is deeper compared to the case of first-year sea ice.

Dyadic coefficient $\bar{\bar{S}}_n$ does not depend on the size of the inclusions but dots depend on ratios of ellipsoidal axial lengths and the orientation distribution of the non-spherical scatterers [*Nghiem et* al., *1993b*]. Physically, it is the shape and orientation that determine the polarizability of the inclusions. Thus, the ellipsoidal shape and orientation of brine inclusions (Section 2.2) are manifested in electromagnetic properties of sea ice even in the lowest order.

The second term in (1) accounts for the wave scattering effect in sea ice. This term depends on frequency; therefore, the inhomogeneous sea ice is inherently dispersive (even if one assumes frequency independence for the constituent permittivities). In the existence of inhomogeneities, wave speed is modified and wave attenuation is increased due to the scattering loss. Effective dyadic scatterer $\bar{\bar{\xi}}_{n\,eff}$ in the second term of (1) is calculated with

$$[\bar{\bar{\xi}}_{neff}]_{jm} = \int_0^\pi \psi_{nf} \int_0^{2\pi} d\phi_{nf}\, p_n(\psi_{nf}, \phi_{nf})$$

$$\sum_{k,l}^{x,y,z} \Gamma^{(0)}_{n\xi jklm} \left\{ k_0^2 \int_{-\infty}^{\infty} d\bar{k}' \, [\overline{\overline{G}}_{ng}(\bar{k}')]_{kl} \Phi_{n\xi}(\bar{k}') + [\overline{\overline{S}}_n]_{kl} \right\} \Bigg|_{\psi_{nf},\phi_{nf}} \tag{3}$$

in which k_0 is the wave number in air, $\overline{\overline{G}}_{ng}$ is the Green's function, $\Gamma^{(o)}_{n\xi jklm}$ is the variance, $\Phi_{n\xi}$ is the Fourier transform of the normalized local correlation function $R_{n\xi}$, and $p(\psi_{nf},\phi_{nf})$ is the probability density function of orientation with Eulerian angles ψ_{nf} and ϕ_{nf} relating the local scatterer coordinates to the global coordinates (x,y,z). Subscript ξ is used to indicate that $\Gamma^{(0)}_{n\xi jklm}$ belongs to $\Phi_{n\xi}$. The variance $\Gamma^{(0)}_{n\xi jklm}$ has the same functional dependence as in (2) and thus the same physical relationship to sea ice properties.

For orientation distributions, $p_n(\psi_{nf},\phi_{nf}) = \sin(\psi_{nf})/(4\pi)$ describes random orientations of scatterers such as ice grains in snow and $p_n(\psi_{nf},\phi_{nf}) = \delta(\psi_{nf})/(2\pi)$ depicts brine inclusions oriented in the vertical direction (delta δ function of ψ_n) in columnar ice with random c-axes in the horizontal plane. The ensemble average over random orientations in snow leads to an isotropic effective permittivity. For the sea ice, the effective permittivity is vertically uniaxial in conformance with the preferential alignment of brine inclusions.

The integration over the product of the Green's function and the correlation function depends on inclusion sizes; therefore, the size effect appears in the higher order compared to the shape and orientation effects. A normalized local correlation function is used to model the ellipsoidal brine inclusions in sea ice. In the local coordinates (x', y', z') associated with the principal axes of an ellipsoid, the correlation function is

$$R_{n\xi}(\bar{r}') = \exp\left[- \left(\frac{x'^2}{\ell_{nx'}^2} + \frac{y'^2}{\ell_{ny}^2} + \frac{z'^2}{\ell_{nz'}^2} \right)^{\frac{1}{2}} \right] \tag{4}$$

with correlation length $\ell_{nx'}, \ell_{ny'}$, and $\ell_{nz'}(n=2)$, related to the effective size and shape of the scatterers [*Nghiem et* al., *1993 b*]. For spheroidal scatterers such as ice grains in the snow layer $(n=1)$, the correlation function is reduced from (4) with $\ell_{nx'} = \ell_{ny'} \equiv \ell_{n\rho'}$.

After substituting correlation function (4) into (3), the integrations are carried out

over the complex integrands for $\overline{\overline{\xi}}_{neff}$ to obtain effective permittivity $\overline{\overline{\epsilon}}_{neff}$ from (1). Expressions for effective permittivities with spheroidal and ellipsoidal scatterers are reported by Yuch et al. [*1990*] and Nghiem et al. [*1993a, 1993b*]. Note that for sea ice ($n = 2$) composed of ice and brine, fractional volumes of the constituents are related by $f_{2ice} = 1 - f_{2brine}$. In this case, Nghiem et al. [1993b] use the notation with subscript s for the scattering brine ($f_{2s} = f_{2brine}$ and $\epsilon_{2s} = \epsilon_{2brine}$) and subscript b for the background ice ($f_{2b} = 1 - f_{2s}$ and $\epsilon_{2b} = \epsilon_{2ice}$). In these calculations, appropriate branch cuts and Riemann sheets are considered for the involving functions with complex variables. The result for ellipsoidal scatterers can be reduced to the case of spheroids by equating two of the three correlation lengths. For randomly oriented scatterers, the effective permittivity becomes isotropic and $\overline{\overline{\epsilon}}_{neff}$ is the unit dyad $\overline{\overline{I}}$ multiplied by a scalar permittivity ϵ_{neff}.

3.2 Volume Inhomogeneities in Layered Media

Inhomogeneities in sea ice, besides influencing wave propagation as presented in Section 3.1, give rise to wave scattering from sea ice into the upper media, Scatterers such as ice grains in the snow layer also contribute to the scattered fields. Thus, physical and structural properties of sea ice are related to both wave propagation and scattering with interactions to the cover layer,

These processes are included in the polarimetric model with the analytic wave theory applied to the layered configurate ion in Figure 6. Scattering sources, due to the permittivity contrasts of the constituents in the inhomogeneous media, are introduced in wave equations for the layered media, Scattered fields are solved from these equations under the distorted Born approximation [*Tsang and Kong, 1981*] with effective permittivities and dyadic Green's functions accounting for wave interactions in the media. The set of sea ice characterization parameters used in the calculation of effective permittivities are utilized in the derivation of the scattered fields. Wave propagation, attenuation, and scattering are therefore consistently linked to sea ice characteristics.

Scattered fields from sea ice are measured in the backscattering direction with a polarimetric scatterometer or radar for all combinations in the linear polarization basis. Ensemble averages of scattered field correlations are used to obtain the complete set of polarimetric backscattering coefficients. These coefficients constitute a covariance matrix or a Mueller matrix, characterizing polarimetric scattering properties of the layered media [*Nghiem et al.,1990*]. To derive the scattering coefficients, operator L_{njklm} is defined as

$$L_{njklm} = \sum_{i,j,k,l,m}^{x,y,z} k_0^4 \int_0^\infty dd_n \, q_n(d_n) \int_0^\pi d\psi_{nf} \int_0^{2\pi} d\phi_{nf} \, p_n(\psi_{nf}, \phi_{nf})$$

$$\int_{V_n} d\bar{r}_n \int_{V_n} d\bar{r}_n^o \, C_{n\xi jklm}(\bar{r}_n, \bar{r}_n^o; \psi_{nf}, \phi_{nf}) \qquad (5)$$

where q_n is the 'probability density function of thickness d_n, p_n is the probability density function of orientation, and location $\bar{r}_n$ or $\bar{r}_n^o$ is in volume V_n occupied by Region n. The orientation distributions are the same as discussed in Section 3.1 for effective permittivity. The thickness distribution characterized by q_n is governed by a first-order differential equation depending on sea ice growth rate, motion, and a redistribution function related to ice deformation [*Thorndike et al., 1975*],

The correlation function $C_{n\xi jklm}$ of the scatterer with variance $_{i',j}$ $_{klm}$ is determined by the following expression

$$C_{n\xi jklm}(\bar{r}_n, \bar{r}_n^o; \psi_{nf}, \phi_{nf}) = \left\langle \xi_{njk}(\bar{r}_n)\xi_{nlm}^*(\bar{r}_n^o) \middle| \psi_{nf}(\bar{r}_n), \phi_{nf}(\bar{r}_n) \right\rangle$$

$$= \int_{-\infty}^\infty d\bar{\beta} \, \Gamma_{njklm} \Phi_{n\xi}(\bar{\beta}) e^{-i\bar{\beta} \cdot (\bar{r}_n - \bar{r}_n^o)} \qquad (6)$$

where $\Phi_{n\xi}$ is the Fourier transform of (4) and ξ_{njk} is the local scatterer [*Nghiem et al., 1993a, 1993b*].

The operator (5) is applied on elements $\langle G \rangle$ of mean dyadic Green's functions and mean incident fields $\langle F \rangle$ to obtain the correlations of scattered fields under the distorted Born approximation as follows

$$\left\langle \overline{E}_{0s}(\bar{r}) \cdot \overline{E}_{0s}^*(\bar{r}) \right\rangle = \sum_{n=1}^2 L_{njklm} \, \left[\left\langle G_{0nij}(\bar{r}, \bar{r}_n) \right\rangle \left\langle F_{nk}(\bar{r}_n) \right\rangle \right]$$

$$\left[\left\langle G_{0nil}(\bar{r}, \bar{r}_n^o) \right\rangle \left\langle F_{nm}(\bar{r}_n^o) \right\rangle \right] * \qquad (7)$$

This result includes the physical and structural properties of the anisotropic sea ice, wave interaction with' the medium interfaces, and effects of the cover layer. The results given by *(7)* can be reduced for application to a simpler sea ice configuration without the cover layer by setting thickness d_1 to zero.

The mean dyadic Green's function $\langle \overline{\overline{G}}_{0n} \rangle$ in (7) is for the observation point in Region O and the source point in Region n. The Green's function has been derived for anisotropic medium in a two-layer configuration [Lee *and Kong, 1983*] and extended for application to a polarimetric model of layered geophysical media [*Nghiem et* al., 1990]. The dyadic Green's function in the radiation field can be written as

$$\langle \overline{\overline{G}}_{0n}(\overline{r},\overline{r}_s) \rangle = \frac{e^{ik_0 r}}{4\pi r} e^{-i\overline{k}_\rho \cdot \overline{\rho}_s} \overline{\overline{g}}_n(\overline{k}_\rho, z_s) \ , \ ?2 \ = \ 1,2 \tag{8}$$

where $e^{ik_0 r}/(4\pi r)$ is the spherical radiation, $\overline{k}_\rho$ is the lateral wave vector, and $\overline{\rho}_s = \hat{x}x_s + \hat{y}y_s$. Dyadic coefficient $\overline{\overline{g}}_n(\overline{k}_\rho, z_s)$ is defined as

$$\overline{\overline{g}}_n(\overline{k}_\rho, z_s) = \sum_\mu \sum_\nu \hat{\mu}(k_{0z}^u) \Big[D_{n\mu\nu}(-\overline{k}_\rho)\hat{\nu}(k_{nz}^{\nu u})e^{-ik_{nz}^{\nu u} z_s}$$
$$+ U_{n\mu\nu}(-\overline{k}_\rho)\hat{\nu}(k_{nz}^{\nu d})e^{-ik_{nz}^{\nu d} z_s} \Big] \tag{9}$$

where polarization unit vector $\hat{\mu}$ can be $\hat{h}$ or $-\hat{v}$, script μ stands for horizontal h or vertical v polarization, and superscripts u and d respectively denote upgoing and downgoing directions. In Region 1, unit vector $\hat{\nu} = \hat{h}, -\hat{v}$ and script u $= h, v$ without a minus sign in front of v. Since Region 1 is isotropic, there is no distinction in the propagation of horizontal or vertical wave; thus, $k_{1z}^{hu} = k_{1z}^{vu} \equiv k_{1z}^u$ and $k_{1z}^{hd} = k_{1z}^{vd} \equiv k_{1z}^d$. In Region 2, the medium can be anisotropic and characteristic waves are ordinary o or extraordinary e. In this case, unit vector $\hat{\nu} = \hat{o}, -\hat{e}$ and script $\nu = $ o, e. There are four types of waves in Region 2: ordinary downgoing, ordinary upgoing; extraordinary downgoing, and extraordinary upgoing. Thus the birefringent effect (double refraction), wave speed difference, and differential attenuation in the anisotropic sea ice medium are accounted for in this model. All polarization and wave vectors are defined by Nghiem et al. [*1990*] and *U's* and *D*'s will be shown later.

For incident field $\overline{E}_{0i} = \left[\hat{h}(k_{0zi})E_{hi} + \hat{v}(k_{0zi})E_{vi}\right]e^{i\overline{k}_{0i}\cdot\overline{r}}$, the mean fields can be written as

$$\left\langle \overline{F}_n(\overline{r}) \right\rangle = e^{\overline{k}_{\rho i}\cdot\overline{\rho}}\,\overline{P}_n(\overline{k}_{\rho i},\, z)\,, \quad n = 1, 2 \tag{1o}$$

where subscript i indicates the incident wave, $\overline{\rho} = \hat{x}x + \hat{y}y$ is the lateral spatial vector, and $\overline{k}_{\rho i} = \hat{x}k_{xi} + \hat{y}k_{yi} = k_0(\hat{x}\sin\theta_{0i}\cos\phi_{0i} + \hat{y}\sin\theta_{0i}\sin\phi_{0i})$ is the lateral component of incident wave vector $\overline{k}_{0i}$, θ_{0i} is the incident angle, and ϕ_{0i} is the azimuthal angle. Polarization vector $\overline{P}_n(\overline{k}_{\rho i}, z)$ is expressed as follows

$$\overline{P}_n(\overline{k}_{\rho i}, z) = \sum_\mu \sum_\nu E_{\mu i}\left[D_{n\mu\nu}(\overline{k}_{\rho i})\hat{v}(k_{nzi}^{\nu d})e^{ik_{nzi}^{\nu d}z}\right.$$
$$\left. + U_{n\mu\nu}(\overline{k}_{\rho i})\hat{v}(k_{nzi}^{\nu u})e^{ik_{nzi}^{\nu u}z}\right] \tag{11}$$

where $\mu = h, v$ and $\nu = h, v$ in Region 1 or $\nu = $ o, e in Region 2, As indicated in (11), the incident wave is effectively decomposed into the ordinary and extraordinary waves in the anisotropic columnar sea ice.

Coefficients U's and D's are derived from boundary conditions. To illustrate the wave interaction processes described by U's and D's, consider amplitude vector $\overline{A}_n$ of upgoing waves and $\overline{B}_n$ of downgoing waves in Region $n = $ O, 1, 2, 3. Amplitude vectors of waves propagating away and toward each interface, as shown in Figure 7, are related with matrix equations

$$\begin{bmatrix} \overline{A}_n \\ \overline{B}_{(n+1)} \end{bmatrix} = \begin{bmatrix} \overline{\overline{R}}_{n(n+1)} & \overline{\overline{T}}_{(n+1)n} \\ \overline{\overline{T}}_{n(n+1)} & \overline{\overline{R}}_{(n+1)n} \end{bmatrix}_H \begin{bmatrix} \overline{B}_n \\ \overline{A}_{(n+1)} \end{bmatrix}_1 \tag{12}$$

In Region O, $\overline{B}_0$ is the amplitude vector of the incident wave, In Region 3, there is no upgoing wave and $\overline{\overline{R}}_{32}$ and $\overline{\overline{T}}_{32}$ are not needed. Amplitude vectors in different layers can be related to the incident vector $\overline{B}_0$ by

$$\overline{A}_n = \overline{\overline{U}}_n \cdot \overline{B}_0 \tag{13a}$$

$$\overline{B}_n = \overline{\overline{D}}_n \cdot \overline{B}_0 \tag{13b}$$

Elements in $\overline{\overline{U}}_n$ are $U_{n\mu\nu}$ and in $\overline{\overline{D}}_n$ are $D_{n\mu\nu}$ where μ and ν can be h or v except that $\nu = $ o, e in Region 2. Matrix $\overline{\overline{U}}_0$ is defined as the reflection matrix $\overline{\overline{R}}_0$ for Region O and $\overline{\overline{D}}_3$

is the transmission matrix $\overline{\overline{T}}_3$ for Region 3. From the system of matrix equations in (12), downgoing and upgoing amplitude vectors are solved in terms of $\overline{B}_0$ and the results are then compared to (13) to obtain coefficient matrices in the dyadic Green's functions and the polarization vectors. Physically, these vectors and matrices describe wave interactions with the interfaces including multiple reflections and transmissions in the sea ice and the cover layer (such as snow, slush, 'or brine), the reflection to the upper air, and the transmission to the underlying sea water.

By applying operator L from (5) on the dyadic Green's functions of the layered media and the mean fields as in (7), correlations of the scattered fields are obtained. Then, polarimetric backscattering coefficients, $\sigma_{\mu\tau\nu\kappa}$, are calculated with

$$\sigma_{\mu\tau\nu\kappa} = \lim_{\substack{r\to\infty \\ A\to\infty}} \frac{4\pi r^2}{A} \frac{\langle E_{\mu s}\, E_{\nu s}^* \rangle}{E_{\tau i}\, E_{\kappa i}^*} \tag{14}$$

where subscripts μ, ν, τ, and κ can be h or v, subscripts i and s respectively stand for incident and scattered fields, r is the distance from the radar, and A is the illuminated area. Coefficients from the dyadic Greens's functions and mean fields are combined to arrive at the following expression of the scattering coefficients in the scattered polarization basis

$$\sigma_{\mu\tau\nu\kappa} = \pi k_0^4 \sum_{n=1}^{2} \int_0^\infty dd_n\, q_n(d_n) \int_0^\pi d\psi_{nf} \int_0^{2\pi} d\phi_{nf}\, p_n(\psi_{nf}, \phi_{nf})$$
$$\sum_{a,b,c,d} \sum_{j,k,l,m}^{x,y,z} \Psi_{n\mu\tau,jk}^{ab} \Psi_{n\nu\kappa,lm}^{cd*} \mathcal{T}_{njklm}^{abcd} \tag{15}$$

in which $a, b = -1, 1$ for n = 1 and $a,\, b, c, d = ou, od, eu, ed$ for $n = 2$.

In (15), the contribution from the isotropic Region 1 (n = 1) consists of 16 terms for downgoing and upgoing incident and scattered waves. In Region 2, 4 wave types in the Green's function and 4 in the incident fields provide 16 terms, which are correlated with 16 terms in the scattered waves giving rise to 256 terms from the sea ice layer, accounting for all types of wave interactions in the anisotropic layered media. Details of Ψ_n's and $\mathcal{T}_n$'s are given by Nghiem et al. [1990, 1993b]. The integrations over Eulerian angles in

(15) can be carried out numerically, When the low-frequency condition is valid, analytical expressions can be derived, For a given thickness distribution, the integration over the thickness probability density function gives the polarimetric scattering coefficients, For a uniform thickness, q_n becomes a Dirac delta function of thickness and the results are readily obtained.

Constituents of sea ice are non-magnetic (Section 2.1) and thus the medium is reciprocal. The cover layer and the underlying sea water are also reciprocal. The reciprocity reduces the backscattering covariance matrix to a 3 x 3 complex Hermitian matrix. In the covariance matrix, conventional backscattering coefficients $\sigma_{hh} \equiv \sigma_{hhhh}$, $\sigma_{vv} \equiv \sigma_{vvvv}$, and $\sigma_{hv} \equiv \sigma_{hvhv}$ are the diagonal elements. The cross-correlation coefficients are σ_{hhhv} and σ_{hvvv}, The co-polarized ratio is defined as $\gamma = \sigma_{vv}/\sigma_{hh}$, the cross-polarized ratio is $e = \sigma_{hv}/\sigma_{hh}$, and the complex correlation coefficient between the horizontal and vertical returns is $\rho = \sigma_{hhvv}(\sigma_{hh}\,\sigma_{vv})^{-1/2}$.

In sea ice where c-axes have random orientations in azimuthal directions, the reflection symmetry completely decorrelates the cross-terms $(\sigma_{hhhv} = \sigma_{hvvv} = 0)$ and the covariance matrix for sea ice contains only 5 independent parameters at oblique incident angles [*Nghiem* et al., 199c] . In (9) and (11), k_{2z}^{od} and k_{2z}^{ou} are different from k_{2z}^{ed} and k_{2z}^{eu} in both real and imaginary parts in the uniaxial sea ice, Consequently, the scattering centers of horizontal and vertical waves are separated because of different wave speeds and attenuations. Then, p calculated from the scattering coefficients with (15) has a reduction in magnitude and an increase in absolute phase compared to the isotropic case. At the normal incident angle, the covariance matrix has 2 independent parameters since $\gamma = 1$, Im $\rho = 0$, and e = $(1 - \rho)/2$ due to the azimuthal symmetry [*Nghiem et al.*, 1992]. These relations in polarimetric coefficients of sea ice are followed by (15). When c-axes are aligned by a sea current, sea ice becomes a biaxial medium, which is not treated in this paper; the polarization signature of a biaxial sea ice is generally characterized by a covariance matrix with 9 independent parameters.

Effects of a cover layer with different compositions and characteristics such as snow, slush, or brine (Section 2.5) on polarimetric signatures of sea ice can be seen from the results in this section. For snow covered sea ice, (15) is the sum for the scattering from snow ($n = 1$) and sea ice ($n = 2$). Due to the isotropy, horizontal and vertical returns from snow are better correlated, The overall effect increases the magnitude of ρ and decrease the absolute value of the phase compared to the case of bare ice. These polarimetric characteristics approach the behavior of an inhomogeneous isotropic medium and thus the anisotropy of the underneath sea ice is partially masked.

When sea ice is covered by a high permittivity layer such as slush or brine, wave attenuation is increased because of the highly lossy salinity. Furthermore, magnitudes of the elements in $\overline{R}_{01}$ increase and the difference between the horizontal and vertical co-polarized elements, $R_{01\,hh}$ and R_{01vv}, are larger especially at larger incident angles. In this case, backscattering coefficients decrease and co-polarized ratio γ increases at larger incident angles. Further complexity is introduced by rough interfaces in sea ice, which are considered in the next section.

3.3 Rough Interfaces in Layered Media

Natural interfaces in sea ice are rough with various length scales (Section 2.5). In this section, surface scattering from rough interfaces in layered media is presented for small scale roughnesses with small standard deviation heights and slopes; large scale roughness such as hummocks are examined later, To estimate effects of rough interfaces on polarimetric signatures of sea ice, contributions from the rough surface scattering are considered with wave interactions, differential propagation delay, and wave attenuations in the anisotropic layered media.

As depicted in Figure 8, the incident wave is scattered by the rough interface between air and snow. The wave continues propagating into the snow layer (Region 1) where both the coherent and incoherent fields are scattered again by ice grains and the rough snow-ice

interface. Part of the wave is transmitted into the ice layer (Region 2) and is further scattered by brine inclusions in this layer and by the rough ice-water boundary. The wave also reflects back towards the top interface and is scattered again by the inhomogeneities and the rough surfaces. This process of multiple scattering is complicated and involves the surface scattering from above and below the interfaces, multiple volume scattering in the inhomogeneous layers, higher-order interactions between volume and surface scattering mechanisms, and wave propagation and attenuation in the multi-layered anisotropic inhomogeneous media. Estimation of rough surface effects here is simplified by considering the first order scattering of the down-going incident field and the higher-order scattering is ignored.

For the top interface, the first-order polarimetric backscattering covariance matrix seen in Region 0 is

$$\overline{\overline{C}}_{01} = \begin{bmatrix} \sigma^{(0)}_{01hhhh} & 0 & \sigma^{(0)}_{01hhvv} \\ 0 & \sigma^{(0)}_{01hvhv} & 0 \\ \sigma^{(0)}_{01vvhh} & 0 & \sigma^{(0)}_{01vvvv} \end{bmatrix} \tag{16}$$

is added to the total scattering [*Lee* and *Kong, 1985*], implying the volume and surface scattered fields are not correlated. Rough surface backscattering coefficients $\sigma^{(0)}_{01hhhh}$ and $\sigma^{(0)}_{01vvvv}$ can be computed with the Kirchhoff approximation, geometric optics approximation, or small perturbation method [*Tsang et al., 1985*]. Under these approximations, cross-polarized return $\sigma^{(0)}_{01hvhv}$ is zero and correlation term $\sigma^{(0)}_{01hhvv} = \sigma^{(0)}_{01vvhh} = [\sigma^{(0)}_{01hhhh}\sigma^{(0)}_{01vvvv}]^{1/2}$.

For the rough surface at the middle interface between snow and ice, wave propagation and attenuation in the layered media are considered, The matrix method with wave vectors *in* Section *(3.2)* is employed in the derivation of surface scattering with wave interactions in layered media. Instead of using $(\overline{k}_{\rho i}$) and $(\overline{k}_{\rho})$ to denote coefficients corresponding to incident and scattered waves, subscript i is used for incident and s for scattered as short-hand notations. As illustrated in Figure 7, incident wave amplitude $\overline{B}_1$ in Region 1 is transmitted from Region O by matrix $\overline{\overline{D}}_{1i}$ operating on $\overline{B}_0$ in Region 1; explicitly,

$\overline{B}_1 = \overline{\overline{D}}_{1i} \cdot \overline{B}_0$. Then, $\overline{B}_1$ is scattered by the rough surface characterized by $\overline{\overline{S}}_{12}$ which renders scattered wave amplitude Al $= \overline{\overline{S}}_{12} \cdot \overline{B}_1$. Scattered wave $\overline{A}_1$ goes upward from Region 1 into Region O by transmission matrix $\overline{\overline{T}}_{10s}$ through the air-snow interface; thus, $\overline{A}_0 = \overline{\overline{T}}_{10s} \cdot \overline{A}_1$. The phase factor and attenuation in Region 1 of thickness d_1 (see Figure 6) can be expressed in the backscattering direction as $\exp(i\overline{k}_{1i} \cdot \overline{r}_{1i}) \exp(i\overline{k}_{1s} \cdot \overline{r}_{1s}) = \exp[i2(k_{\rho i}\rho + k^u_{1ziR}d_1)] \exp(-2k^u_{1ziI}d_1)$ where ρ is the lateral distance and scripts ρ, z, R, I, and u stand for the lateral component, vertical component, real part, imaginary part, and up-going direction, respectively. Under consideration of wave propagation, attenuation, and interactions, surface backscattering due to the middle interface observed in Region O is described by

$$\overline{\overline{S}}^{(0)}_{12} = T_{10s}\overline{\overline{T}}.7712 \cdot \overline{D}_{1i} \, e^{i2(k_{\rho i}\rho + k^u_{1ziR}d_1)} e^{-2k^u_{1ziI}d_1} \tag{17}$$

In the anisotropic layered configuration with vertical optic axis under the aforementioned approximations in the derivation of rough surface scattering, horizontal and vertical waves are decoupled and the cross-polarized returns vanish. For the observation in Region O, non-zero elements of the covariance matrix $\overline{\overline{C}}_{12}$ obtained from (17) for the backscattering from the rough interface between Regions 1 and 2 are

$$\sigma^{(0)}_{12hhhh} = (T_{10hhs}D_{1hhi}S_{12hh})(T_{10hhs}D_{1hhi}S_{12hh})^* e^{-4k^u_{1ziI}d_1}$$
$$= |T_{10hhs}D_{1hhi}|^2 e^{-4k^u_{1ziI}d_1}\sigma_{12hhhh} \tag{18a}$$

$$\sigma^{(0)}_{12vvvv} = (T_{10vvs}D_{1vvi}S_{12vv})(T_{10vvs}D_{1vvi}S_{12vv})^* e^{-4k^u_{1ziI}d_1}$$
$$= |T_{10vvs}D_{1vvi}|^2 e^{-4k^u_{1ziI}d_1}\sigma_{12vvvv} \tag{18b}$$

$$\sigma^{(0)}_{12hhvv} = (T_{10hhs}D_{1hhi}S_{12hh})(T_{10vvs}D_{1vvi}S_{12vv})^* e^{-4k^u_{1ziI}d_1}$$
$$= (T_{10hhs}D_{1hhi})(T_{10vvs}D_{1vvi})^* e^{-4k^u_{1ziI}d_1}\sigma_{12hhvv} \tag{18c}$$

where σ_{12hhhh}, σ_{12vvvv}, and $\sigma_{12hhvv} = (\sigma_{12hhhh}\sigma_{12vvvv})^{1/2}$ are polarimetric backscattering coefficients for the rough surface. In the calculation of $\sigma_{12\mu\nu\tau\kappa}$, incident angle θ_{1i} in Region

1 is determined by $\theta_{1i} = \tan^{-1}(k_{\rho i}/k_{1ziR})$ duc to the phase matching conditions. Under the Kirchhoff or geometric optics approximation, the Fresnel reflection coefficient at the interface is evaluated at normal incidence without distinguishing horizontal or vertical wave polarization. In the small perturbation method, the two wave types arc treated differently. Since Region 2 is vertically uniaxial, the reflection coefficient is computed with ordinary wave for horizontal polarization and extraordinary wave for vertical polarization,

Scattering coefficients of the rough surface at the bottom interface between ice and water are derived in a similar manner. Incident wave amplitude $\overline{B}_0$ in Region O transmits into Region 2 as $\overline{B}_2 = \overline{\overline{D}}_{2i} \cdot \overline{B}_0$. This incident wave then undergoes the scattering characterized by $\overline{\overline{S}}_{23}$ from the rough interface between Regions 2 and 3, Scattered wave $\overline{A}_2 = \overline{\overline{S}}_{23} \cdot \overline{B}_2$ is observed in Region O as $\overline{A}_0 = \overline{\overline{U}}_s$ .22. Matrix $\overline{\overline{U}}_s$ is derived by considering wave transmission and reflection in the layered configuration. Wave amplitude vector $\overline{A}_1$ is transmitted into Region O as $\overline{A}_0 = \overline{\overline{T}}_{10s} \cdot \overline{A}_1$ where $\overline{A}_1$ in Region 1 is composed of the reflection $\overline{\overline{R}}_{12s} \cdot \overline{B}_1$ from the interface between regions 1 and 2 and the transmission $\overline{\overline{T}}_{21s} \cdot \overline{A}_2$ from Region 2. Thus, $\overline{A}_1 = \overline{\overline{R}}_{12s} \cdot \overline{B}_1 + \overline{\overline{T}}_{21s} \cdot \overline{A}_2$ which relates $\overline{A}_1$ to $\overline{A}_2$ as $\overline{A}_1 = (\overline{\overline{I}} - \overline{\overline{R}}_{12s} \cdot \overline{\overline{R}}_{10s})^- A_2^-$ where $\overline{\overline{I}}$ is the identity matrix. By operating $\overline{\overline{T}}_{10s}$ on $\overline{A}_1, \overline{A}_0$ is obtained in terms of $\overline{A}_2$ and $\overline{\overline{U}}_s$ is identified as

$$\overline{\overline{U}}_s = \overline{\overline{T}}_{10s} \cdot (\overline{\overline{I}} - \overline{\overline{R}}_{12s} \cdot \overline{\overline{R}}_{10s})^{-1} \ .721. \ \equiv \begin{bmatrix} U_{ohs} & U_{ovs} \\ U_{ehs} & U_{evs} \end{bmatrix} \tag{19}$$

where o denotes ordinary wave and e is for extraordinary wave.

In the vertical uniaxial layered configuration, horizontal and vertical components are decoupled. In this case, the necessary elements U_{ohs} and U_{evs} are obtained from (19) and expressed as

$$U_{ohs} = \frac{e^{i(k_{1zs} - k_{2zs}^o)d_1} T_{21oh} T_{10hh}}{1 - e^{i2k_{1zs}d_1} R_{12hh} R_{10hh}^-} \tag{20a}$$

$$u_{evs} = \frac{e^{i(k_{1zs} - k_{2zs}^{eu})d_1} T_{21ev} T_{10vv}}{1 - e^{i2k_{1zs}d_1} R_{12vv} R_{10vv}} \tag{20b}$$

where $k_{2zs}^o \equiv k_{2zs}^{ou} = -k_{2zs}^{od}$. Furthermore, wave propagation in Region 2, whose interface with Region 3 locates at the depth of d_2, *imposes on* the backscattered wave a phase factor

and attenuation of

$$e^{i\overline{k}_{2oi}\cdot\overline{r}_{2i}}e^{i\overline{k}_{2os}\cdot\overline{r}_{2s}} = e^{i2k_{\rho i}\rho_c}e^{i(k^o_{2zsR}+k^o_{2ziR})(d_2-d_1)}$$

$$e^{-(k^o_{2zsI}+k^o_{2ziI})(d_2-d_1)} \tag{21a}$$

$$e^{i\overline{k}_{2ei}\cdot\overline{r}_{2i}}e^{i\overline{k}_{2es}\cdot\overline{r}_{2s}} = e^{i2k_{\rho i}\rho_c}e^{i(k^{eu}_{2zsR}-k^{ed}_{2ziR})(d_2-d_1)}$$

$$e^{-(k^{eu}_{2zsI}-k^{ed}_{2ziI})(d_2-d_1)} \tag{21b}$$

for ordinary and extraordinary waves, respectively,

After wave propagation and multiple interactions with boundaries in the anisotropic layered media are considered, the covariance matrix observed in Region O has the following non-zero elements in terms of backscattering coefficients derived from (20) and (21) for the rough interface between Regions 2 and 3

$$\sigma^{(0)}_{23hhhh} = |U_{ohs}D_{2hoi}|^2 e^{-2(k^o_{2zsI}+k^o_{2ziI})(d_2-d_1)}$$

$$e^{-2(k_{1zsI}+k_{1ziI})d_1}\sigma_{23hhhh} \tag{22a}$$

$$\sigma^{(0)}_{23vvvv} = |U_{evs}D_{2vei}|^2 e^{-2(k^{eu}_{2zsI}-k^{ed}_{2ziI})(d_2-d_1)}$$

$$e^{-2(k_{1zsI}+k_{1ziI})d_1}\sigma_{23vvvv} \tag{22b}$$

$$\sigma^{(0)}_{23hhvv} = (U_{ohs}D_{2hoi})(U_{evs}D_{2vei})^*$$

$$e^{i(k^o_{2zsR}+k^o_{2ziR}-k^{eu}_{2zsR}+k^{ed}_{2ziR})(d_2-d_1)}$$

$$e^{-(k^o_{2zsI}+k^o_{2ziI}+k^{eu}_{2zsI}-k^{ed}_{2ziI})(d_2-d_1)}$$

$$e^{-2(k_{1zsI}+k_{1ziI})d_1}\sigma_{23hhvv} \tag{22c}$$

Under the Kirchhoff, geometric optics, or small perturbation approximations, $\sigma_{23hhvv} = (\sigma_{23hhhh}\sigma_{23vvvv})^{1/2}$. In the calculation of the scattering from the interface between Regions 2 and 3, the ordinary wave reflection coefficient is used for horizontal polarization and extraordinary wave for vertical polarization, Incident angles in Region 2 for ordinary and extraordinary waves are respectively determined by $\theta_{2oi} = \tan^{-1}(k_{\rho i}/k^o_{2ziR})$ and $\theta_{2ei} = \tan^{-1}(-k_{\rho i}/k^{ed}_{2ziR})$. Note that there is an extra phase term in $\sigma^{(0)}_{23hhvv}$ (22c) due to the difference in propagation speeds of ordinary and extraordinary waves.

Surface scattering dominates the total backscattering at small incident angles where the information carried by the scattering from the underneath ice layer is masked out of polarimetric signatures. Surface scattering depends on the roughness and the permittivity contrast between the upper and lower media at the medium interface. For the same roughness, a higher permittivity contrast gives higher backscattering. In snow covered sea ice, the permittivity contrast at the air-snow interface, especially for dry snow, is smaller than that at the snow-ice interface. In this case, the contribution from the snow-ice rough surface is more important and the total sea ice signature carries some information pertaining to this surface.

Roughness at a sea ice interface evolves under many processes related to environmental conditions such as atmospheric boundary layer, winds, sea currents, wave actions, solar radiation and heat transport. These processes create many types of sea ice with complicated surface conditions, compositions, and structures such as composite pancake ice, rafted ice, pressure ridges, puddles and thaw holes, which are subjects of future model developments. In the following sections, melt hummocks, another complication in polarimetric sea ice signatures, are modeled and presented in terms of their effects on both volume and surface scattering mechanisms in sea ice.

3.4 Volume Scattering with Hummock Surface

Multi-year sea ice survives at least one summer season during which differential melt creates hummocks on the ice surface with a large scale roughness of the order of a few meters [*Cox, and Weeks, 1974; Weeks and Ackley, 1982*]. During winter, multi-year ice is covered by a new layer of snow over the hummocks. Both the top interface between air and snow and the middle between snow and ice have this undulating topography.

Evidently, a local incident angle of the electromagnetic wave differs from the global incident angle set by the antenna looking direction. Effects of this meter-scale topography on the volume scattering from the layered media are accounted for by averaging scattering

coefficients over the distribution of local incident angles. This averaging process implies the characteristic length of the hummock topography is large enough so that the local scattering can be treated independently, The method has been applied to composite models for rough surface scattering from small scale roughness with large scale modulation [*Wright, 1968*]. When surface slopes of the upper and lower hummock interfaces are highly correlated with a positive correlation coefficient, the total volume scattering from the layered media can simply be averaged over the distribution of the local incident angles at the top interface, Under this condition, the two interfaces are closely in parallel and their large scale characteristic lengths are similar.

Scattering coefficient $\sigma_{\mu\nu\tau\kappa}^{(V)}$ due to the volume scattering under the effects of the hummock topography is determined by $\sigma_{\mu\nu}^{(V)} = \int \sigma'_{\mu\nu\tau\kappa}(\theta_\ell, \phi_\ell) d\Omega / \int d\Omega$, which is the average of local scattering coefficient $\sigma'_{\mu\nu\tau\kappa}$, evaluated at local incident angle θ_ℓ and azimuthal angle ϕ_ℓ, over the observation solid angle Ω. For the unit vector $\hat{n} = (-\hat{x}\chi - \hat{y}\varphi + \hat{z})/(\chi^2 + \varphi^2 + 1)112$ normal to the local surface and backscattering direction $\hat{k} = (-\hat{x}\sin\theta_{0i}\cos\phi_{0i} - \hat{y}\sin\theta_{0i}\sin\phi_{0i} + \hat{z}\cos\theta_{0i})$ defined by the global incident angle θ_{0i} and azimuthal angle ϕ_{0i}, the average for $\sigma_{\mu\nu\tau\kappa}^{(v)}$ can be written as

$$\sigma_{\mu\nu\tau\kappa}^{(v)} = \iint d\chi d\varphi \, \sigma'_{\mu\nu\tau\kappa}(\theta_\ell, \phi_\ell) \, P(X, \varphi)$$
$$[1 + \tan\theta_{0i}(\chi\cos\phi_{0i} + \varphi\sin\phi_{0i})] \tag{23}$$

in which $P(\chi, \varphi)$ is the probability density function of slope and local incident angle θ_ℓ is

$$\cos\theta_\ell = \hat{k} \cdot \hat{n} = \frac{\cos\theta_{0i} + \sin\theta_{0i}(\chi\cos\phi_{0i} + \varphi\sin\phi_{0i})}{\left(\chi^2 + \varphi^2 + 1\right)^{1/2}} \tag{24}$$

Since the scattering configuration has reflection symmetry with respect to all vertical planes, the azimuthal angle ϕ_{0i} can be set to zero without loss of generality. In this case, the limit of integration for φ is from $-\infty$ to $+\infty$ and for χ is from $-\cot\theta_{0i}$ to $+\infty$. The lower limit $-\cot\theta_{0i}$ is introduced to account for the shadowing effect of the large scale surface [*Chan and Fung, 1977*]. For a Gaussian distribution of slope S $= \sqrt{2}\,\sigma_R/\ell_R$ of

the large scale topography with standard deviat ion height σ_R and correlation length ℓ_R, the slope distribution is $p(\chi, \varphi) = \exp[-(\chi^2 + \varphi^2)/(2S^2)]$ and polarimetric backscattering coefficients under the hummock effects are determined by

$$
\sigma_{\mu\nu\tau\kappa}^{(V)} = \int_{-\cot\theta_{0i}}^{\infty} d\chi \, (1 + \chi \tan\theta_{0i}) \frac{e^{-\chi^2/(2S^2)}}{\pi S^2}
$$
$$
\int_{-\infty}^{\infty} d\varphi \, \sigma_{\mu\nu\tau\kappa}'(\theta_\ell) e^{-\varphi^2/(2S^2)}
\tag{25}
$$

When the local surface is tilted, the incident horizontal polarization is composed of both transverse electric (TE) and transverse magnetic (TM) components. This can be interpreted as a roll of the incident polarization basis by an angle α between the incident horizontal vector $\hat{h}_i = \hat{z} \times \hat{k}_i / |\hat{z} \times \hat{k}_i|$ and the local horizontal polarization $\hat{h}_\ell = \hat{n} \times \hat{k}_i / |\hat{n} \times \hat{k}_i|$ (see Figure 8) for global vertical unit vector $\hat{z}$ and incident unit vector $\hat{k}_i = -\hat{k}$. All scattering coefficients $\sigma_{\mu\nu\tau\kappa}'$ are expressible in terms of $\sin\alpha$ and $\cos\alpha$ [*Nghiem*, 1992a]. For $\phi_{0i} = 0$,

$$
\sin\alpha = (\hat{h}_\ell \times \hat{h}_i) \cdot \hat{k}_i = \frac{-\varphi}{[\varphi^2 + (\sin\theta_{0i} - \chi\cos\theta_{0i})^2]^{1/2}}
\tag{26a}
$$

$$
\cos\alpha = \hat{h}_\ell \cdot \hat{h}_i = \frac{\sin\theta_{0i} - \chi\cos\theta_{0i}}{[\varphi^2 + (\sin\theta_{0i} \chi\cos\theta_{0i})^2]^{1/2}}
\tag{26b}
$$

Locally, all cross-correlations in $\sigma_{\mu\nu\tau\kappa}$ are zero due to the local reflection symmetry. In the global coordinates, all cross-correlation in $\sigma_{\mu\nu\tau\kappa}^{(V)}$ are also expected to be nullified due to the global reflection symmetry [*Nghiem, 1992*]. This can be demonstrated by considering scattering coefficient σ_{hhhv}' instance. After the polarization roll and the reciprocity are used,

$$
\sigma_{hhhv}' = \sin\alpha \cos\alpha \left[-\sigma_{hhhh} \cos^2\alpha + \sigma_{vvvv} \sin^2\alpha + \sigma_{hhvv} \cos^2\alpha \right.
$$
$$
\left. -\sigma_{vvhh} \sin^2\alpha + 2\sigma_{hvhv}(\cos^2\alpha - \sin^2\alpha) \right]
\tag{27}
$$

Since $\sin\alpha$ is an odd function of φ while $\cos\alpha$ is even, the integration over φ renders $\sigma_{hhhv}^{(V)}$ zero when $p(\chi, \varphi)$ is an even function of φ, which is the case for a non-directional slope

distribution of the large scale topography such as the Gaussian distribution. All other cross-correlations in $\sigma^{(v)}_{\mu\nu\tau\kappa}$ are shown to be zero in the same manner. For the calculation of the non-zero $\sigma^{(v)}_{\mu\nu\tau\kappa}$, the necessary local polarimetric scattering coefficients are

$$\sigma'_{hhhh} = \sigma_{hhhh}\cos^4\alpha + \sigma_{vvvv}\sin^4\alpha$$
$$+ (\mathrm{Re}\,\sigma_{hhvv} + 2\sigma_{hvhv})2\cos^2\alpha\sin^2\alpha \tag{28a}$$

$$\sigma'_{vvvv} = \sigma_{vvvv}\cos^4\alpha + \sigma_{hhhh}\sin^4\alpha$$
$$+ (\mathrm{Re}\,\sigma_{hhvv} + 2\sigma_{hvhv})2\cos^2\alpha\sin^2\alpha \tag{28b}$$

$$\sigma'_{hhvv} = \sigma_{hhvv}\cos^4\alpha + \sigma_{vvhh}\sin^4\alpha$$
$$+ (\sigma_{hhhh} + \sigma_{vvvv})\cos^2\alpha\sin^2\alpha$$
$$- 4\sigma_{hvhv}\cos^2\alpha\sin^2\alpha \tag{28c}$$

$$\sigma'_{hvhv} = \sigma_{hvhv}(\cos^2\alpha - \sin^2\alpha)^2$$
$$+ (\sigma_{hhhh} + \sigma_{vvvv} - 2\mathrm{Re}{\sim}hhvv)\mathrm{COS}2Q'\mathrm{Sin}2\theta \tag{28d}$$

As seen in *(28)*, $\sigma'_{\mu\nu\tau\kappa}$ has a contribution from $\sigma_{\mu\nu\tau\kappa}$ with a factor of $\mathrm{Cos}^4\alpha$. Usually, α is small and this term is large compared to the terms involving $\sin\alpha$. Consider the cross-polarized return σ'_{hvhv} (28d) for multi-year sea ice: the term $(\sigma_{hhhh} + \sigma_{vvvv} - 2\mathrm{Re}\,\sigma_{hhvv})$ has the same order of magnitude as σ_{hvhv} [*Nghiem, 1993c*]; therefore, σ'_{hvhv} is dominated by the contribution from the first term in (28d) for small angle α in the trigonometric factors. For large scale hummocks with a long correlation length compared to the standard deviation height, $\sigma'_{\mu\nu\tau\kappa}$ mainly retains the characteristics of $\sigma_{\mu\nu\tau\kappa}$ with *some* polarization mixture from other coefficients. In general, hummock effects on volume scattering are to reduce both polarization and incident angle dependences in sea ice signatures as indicated by (28) and (23).

3.5 Surface Scattering with Hummock Surface

Effects of hummocks on backscattering from rough interfaces can be estimated by

averaging local scattering coefficients over the slope distribution of the large scale topography. If the small scale roughness is valid for the small perturbation method, scattering from small surface pert... bations is first calculated and then averaged over the large scale slope distribution. Then the results are added to the scattering from the large scale roughness obtained under the geometric optics approximation. This approach uses different approximations together and considers small scale roughness being tilted locally over patches of large scale roughness according to the slope distribution of the large surface, In contrast, the method used in this paper considers the small scale and large scale roughnesses at the **same time**, applying the Kirchhoff 's approximation to the total roughness, and calculating the total scattering from the composite surface altogether.

Let the total profile $f = f_r + f_R$ be the superposition of a small scale profile f_r and a hummock profile f_R, which are statistically independent and stationary Gaussian processes. The Gaussian distributions of probability densities for these azimuthally symmetric roughness profiles are prescribed by

$$p_r(f_r) \quad \frac{1}{\sqrt{2\pi}\ \sigma_r} \quad \exp\left(-\frac{f_r^2}{2\sigma_r^2}\right) \tag{29a}$$

$$p_R(f_R) = \frac{1}{\sqrt{2\pi}\ \sigma_R} \exp\left(-\frac{f_R^2}{2\sigma_R^2}\right) \tag{29b}$$

where σ_r and σ_R are the standard deviations of the small scale and the hummock profiles, respectively. Under these conditions, the probability density $p(f)$ of the total roughness profile is a convolution of $p_r(f_r)$ and $p_R(f_R)$ [*Papoulis, 1984*]

$$p(f) \cdot p(f_r + f_R) \cdot \int_{-\infty}^{\infty} df_R\ p_r(f - f_R) p_R(f_R)$$

$$= \frac{1}{\sqrt{2\pi}\ (\sigma_r^2 + \sigma_R^2)} \exp\left[-\frac{f^2}{2(\sigma_r^2 + \sigma_R^2)}\right] \tag{30}$$

which is also a Gaussian distribution whose height variance $\sigma^2 = \sigma_r^2 + \sigma_R^2$ is the sum of the individual variances.

The joint probability density $p(f_1, f_2)$ for two points at $\bar{\rho}_1$ and $\bar{\rho}_2$ on the surface is

[Davenport and Root, 1958]

$$p(f_1, f_2) = \frac{1}{2\pi\sigma^2\sqrt{1-C^2}} \exp \left[- \frac{f_1^2 - 2Cf_1 f_2 + f_2^2}{2\sigma^2(1-C^2)} \right] \tag{31}$$

where C is the normalized correlation function between the two points. For the azimuthally symmetric stationary surface, C depends only on the distance $p' = |\overline{\rho}_1 - \overline{\rho}_2|$. From the total profile $f = f_r + f_R$, C is derived as follows

$$\sigma^2 C(\rho') = < f(\overline{\rho}_1)f(\overline{\rho}_2) > = \sigma_r^2 C_r(\rho') + \sigma_R^2 C_R(\rho') \tag{32}$$

To arrive at *(32)*, the independence between f_r and f_R and the following correlation functions have been used

$$< f_r(\overline{\rho}_1)f_r(\overline{\rho}_2) > = \sigma_r^2 C_r(\rho') = \sigma_r^2 \exp\left(-\frac{\rho'^2}{\ell_r^2}\right) \tag{33a}$$

$$< f_R(\overline{\rho}_1)f_R(\overline{\rho}_2) > = \sigma_R^2 C_R(\rho') = \sigma_R^2 \exp\left(-\frac{\rho'^2}{\ell_R^2}\right) \tag{33b}$$

where ℓ_r is the correlation length of the small scale roughness and ℓ_R is that of the hummock topography, As seen in (32), normalized correlation function C is a linear combination of small scale correlation function C_r and hummock correlation function CR.

For a composite surface, consisting of large scale hummocks and small scale roughness characterized by the above descriptions, polarimetric backscattering coefficients $\sigma_{\mu\nu\tau\kappa}^{(s)}$ are derived with stationary phase method under Kirchhoff's approximation. The results for non-zero backscattering coefficients for the composite rough interface at oblique incident angle θ_i arc

$$\sigma_{\mu\mu\nu\nu}^{(S)} = \frac{k^2|R_0|^2}{\pi\cos^2\theta_i} D \tag{34}$$

in which μ and ν can be h or v polarization, k is the wave number in the upper medium, $|R_0|^2$ is the Fresnel reflectivity between the upper and the lower media at normal incident angle, and the quantity D is defined by

$$D = \int_0^{2\pi} d\phi \int_0^{\infty} d\rho' \, \rho' \left\{ e^{-k_{dz}^2\sigma^2[1-C(\rho')]} - e^{-k_{dz}^2\sigma^2} \right\} e^{ik_{d\rho}\hat{\rho}\cdot\overline{\rho}'} \tag{35}$$

where the subscript d denotes the difference between the incident and scattered wave vectors; thus, $\overline{k}_d = \overline{k}_i - \overline{k}_s = \hat{\rho}k_{d\rho} + \hat{z}k_{dz}$ in the cylindrical coordinates. In the backscattering direction, $k_{d\rho} = 2k^2 \sin\theta_i$ and $k_{dz} = 2k^2 \cos\theta_i$.

Carrying out the integration over azimuthal angle ϕ results in the Bessel function $J_0(k_{d\rho}\rho')$ and then substituting the correlation function $C(\rho')$ from (32) yield

$$D = \pi \sum_{m=1}^{\infty} \left\{ \frac{k_{dz}^{2m}}{m!} e^{-k_{dz}^2\sigma^2} \left[\sum_{j=1}^{m+1} \sigma_r^{2[m-(j-1)]}\sigma_R^{2(j-1)} a_{mj} A_{mj} \right] \right\} \tag{36}$$

where a_{mj} is the binomial coefficient and A_{mj} is an integral over ρ' determined by

$$A_{mj} = 2 \int_0^{\infty} dp' \; \rho' J_0(k_{d\rho}\rho') C_r(\rho')^{m-(j-1)} C_R(\rho')^{(j-1)} = \frac{1}{\nu_{mj}} \exp\left(-\frac{k_{d\rho}^2}{4\nu_{mj}}\right) \tag{37}$$

To obtain the result in (37), (33) has been used for the correlation functions and ν_{mj} has been defined in terms of the correlation lengths as

$$\nu_{mj} = \frac{m - (j-1)}{\ell_r^2} + \frac{j-1}{\ell_R^2} \tag{38}$$

With the above solution, the result for backscattering coefficient $\sigma_{\mu\mu\nu\nu}^{(s)}$ from (34) can be written compactly as

$$\sigma_{\mu\mu\nu\nu}^{(s)} = \frac{k^2|R_0|^2}{\cos^2\theta_i} e^{-k_{dz}^{2m}\sigma^2} \sum_{m=1}^{\infty} \sum_{j=1}^{m+1} (k_{dz}\sigma_{mj})^{2m} \alpha_{mj} A_{mj} \tag{39}$$

where $\alpha_{mj} = (a_{mj}/m!)$ and σ_{mj} are determined by the following equations, respectively

$$\alpha_{mj} = \frac{j}{j![m-(j-1)]!} \tag{40}$$

$$\sigma_{mj} = \sigma_r^{1-(j-1)/m}\sigma_R^{(j-1)/m} \tag{41}$$

The above results for polarimetric backscattering coefficients from rough surfaces under effects of large scale hummocks analytically reduce to the small scale surface scattering when the large scale surface profile is removed by letting $\sigma_R = 0$. Furthermore, the results approach the geometric optics solution in the high frequency limit. At large incident angles, the Kirchhoff results for rough surface scattering becomes less accurate; however, the

surface contribution already becomes small and the volume scattering takes over the total sea ice signatures.

In the layered configuration, wave propagation and multiple interactions with layer boundaries are taken into account as shown in Section 3.3 where $\sigma_{n(n+1)\mu\tau\nu\kappa}$ is replaced by the corresponding $\sigma^{(S)}_{\mu\tau\nu\kappa}$, with σ_R and ℓ_R replaced by $\sigma_{n(n+1)R}$ and $\ell_{n(n+1)R}$ to denote the parameters between medium n and $(n + 1)$, in the calculations of $\sigma^{(0)}_{n(n+1)\mu\tau\nu\kappa}$ observed in Region O. Since the composite interfaces contain different scale lengths, large scale hummocks and small scale roughnesses have different responses at different wave frequencies.

4. SUMMARY AND DISCUSSIONS

This paper presents a composite model for polarimetric signatures of sea ice. The purpose is to relate sea ice physical, structural, and electromagnetic properties and processes to sea ice polarimetric signatures. Based on sea ice characteristics, effective permittivities are derived with the strong permittivity fluctuation theory and polarimetric backscattering coefficients arc obtained with the analytical wave theory under the distorted Born approximation. Surface scattering from rough layer interfaces is also considered with effects of wave attenuation and phase delay in an anisotropic layered configuration for sea ice.

Sea ice is an inhomogeneous medium composed of various dispersive constituents. These constituents are non-magnetic materials preserving the reciprocity in sea ice signatures. In the form of the ordinary ice polymorph, natural polycrystalline ice is composed of multiple ice platelets. These platelets entrap brine in ellipsoidal pockets with preferential vertical alignment, Random orient ations of tryst allographic c-axes in azimuthal directions render sea ice uniaxially anisotropic. The anisotropy causes the effective birefringence, differential phase delay an attenuation in sea ice. Temperature, salinity, and density determine the phase distribution of sea ice constituents, including salt expulsion and brine solid-

ification below the eutectic temperature. From the phase distribution, fractional volumes of sea ice constituents are obtained to derive both effective permittivities and polarimetric scattering coefficients of sea ice. Thus, effective permittivities and scattering coefficients are consistently linked to sea ice characteristics.

Dendritic growth of sea ice forms columnar ice where crystal size and brine volume depend on the growth rate thereby influencing wave propagation, attenuation, and scattering. Desalination processes in sea ice increase wave penetration while weaken local scattering effects due to a low permittivity contrast between air bubbles and ice background. Isotropic snow cover can partially mask the anisotropic characteristics in sea ice signatures. Furthermore, snow affects salinity distributions by brine wicking and consequently changes both effective permittivities and polarimetric coefficients. Slush or brine layer with a large permittivity inflicts large reflection and attenuation, decreases the scattering contribution from the ice layer, and increases the co-polarized ratio at large incident angles.

Effects of roughness are important at small incident angles. Rough surface scattering depends on both roughness and permittivity contrast at the interface. The contribution from a rough interface beneath the ice layer suffers from differential attenuation and phase delay. Hummocks have an averaging effect on polarimetric volume scattering, which mixes local polarization responses and reduces the dependence of sea ice signatures on incident angles. Moreover, hummocks modulate the small scale roughness and the response from the composite interface is frequency dependent. From symmetry properties of sea ice scattering configurations, the number of independent parameters contained in covariance matrices for polarimetric signatures of sea ice are also determined.

Based on physical, structural, and electromagnetic properties and their interrelating processes, the composite model can be used to interpret polarimetric signatures of various ice types. For bare sea ice, the results are obtained simply by setting the thickness of the cover layer to zero. For sea ice in a frozen lead with a brine skim or slush cover, polarimetric

signatures arc calculated with a layered configuration where the ice layer has a thickness distribution and the cover layer has a large effective permittivity determined from its highly saline composition. For snow covered first-year sca ice, signatures obtained from the model with snow and sea ice properties include scattering from snow with spheroidal ice grains, sca ice with ellipsoidal brine inclusions, anisotropy due sea ice structure, wave interactions with boundaries, and rough interface effects in the anisotropic layered sca ice media, For multi-year sea ice, the model accounts for hummocks on the snow covered ice with surface tilting effects and composite rough interfaces.

In the second paper of the series, the model will be used to" interpret measured polarimetric signatures of sea ice in the Beaufort sea. Sea ice characterization data obtained from sca ice expeditions and experiments will be utilized. The trends in experimental data will be explained and the utility of polarimetric signatures for global sea ice monitoring will be discussed. For higher order effects in sca icc signatures and more complicated sea ice types, properties, and processes, further developments in sea ice modeling and measurements are necessary.

REFERENCES

Arconc, S. A., A. J. Gow, and S. G. McGrew, Structure and dielectric properties at 4.8 and 9,5 GHz of saline ice, *J. Geophys.Res.*, 91(C12), 14281-14303, 1986.

Borgeaud, M., S. V. Nghiem, R. T. Shin, and J. A. Kong, "Theoretical Models for Polarimetric Microwave Remote Sensing of Earth Terrain," *J. Electromagn.Waves*

Appl., *3*(1), 61-81, 1989.

Cavalieri, D. J., J. P, Crawford, M. R. Drinkwater, D. T. Eppler, L. D. Farmer, R. R. Jentz, and C. C, Wackerman, Aircraft active and passive microwave validation of sea ice concentration from the Defense Meteorological Satellite Program Special Sensor Microwave Imager, *J. Geophys. Res.*, *96*(C12), *21989-22008, 1991.*

Chan, H. L., and A. K. Fung, A theory of sea scatter at large incident angles, *J. Geophys. Res.*, *82(24), 3439-3444, 1977,*

Cox, G. F. N., and W. F. Weeks, Salinity variations in sea ice, *J. Glaciol.*, *13*(67), *109-120, 1974.*

Cox, G. F. N., and W. F. Weeks, Equations for determining the gas and brine volumes in sea-ice samples, *J. Glaciol.*, 29(12), 306-316, 1983.

Davenport, W. B., Jr., and W. L. Root, *An Introduction to the Theory of Random Signals and Noise*, McGraw-Hill, New-York, 1958.

Drinkwater, M. R, and G. B. Crocker, Modelling changes in the dielectric and scattering properties of young snow-covered sea ice at GHz frequencies, *J. Glaciol.*, **$4(118),** 274-282, 1988.

Eicken, H., Salinity profiles of Antarctic sea ice: Field data and model results, *J. Geophys. Res.*, 97(C1O), 15545-15557, 1992.

Evans, S. , Dielectric properties of ice and snow -- A review, *J. Glaciol.* 5, 773-792, 1965.

Glen, J. W., *The Physics of Ice, Monogr. Ser.,* Vol. II-C2a, U. S. Army Corps of Engineers, Cold Regions Research and Engineering Laboratory, Hanover, New Hampshire, 1974,

Gow, A. J., D. A. Meese, D. K. Perovich, and W. B. Tucker III, The anatomy of a freezing lead, *J. Geophys. Res.*, *95(C1O), 18221-18232,* 1990.

Hobbs, P. V., *Ice Physics,* Clarendon Press, Oxford, 1974.

Klein, L. A., and C. Swift, An improved model for the dielectric constant of sea water at microwave frequencies, *IEEE Trans. Antennas Propagat.*, *AP-25*(1), *104-111, 1977.*

Kong, J. A., *Electromagnetic Wave Theory,* John Wiley, New-York, 1986.

Kwok, R., M. R. Drinkwater, A. Pang, and E. Rignot, Characterization and classification of sea ice on polarimetric SAR data, *International Geoscience and Remote Sensing Symposium;* Vol. II, pp. 81-84, May 26-29, 1991,

Lee, J. K., and J. A. Kong, Dyadic Green's functions for layered anisotropic medium, *Electromag., 3, 111-130, 1983,*

Lee, J. K., and J. A. Kong, Active microwave remote sensing of an anisotropic random medium layer, *IEEE Trans. Geosci. Remote Sens., GE-23, No. 6, 910-923, 1985.*

Lofgren, G., and W. F. Weeks, Effect of growth parameters on substructure spacing in NaCl ice crystal, *J.Glaciol., 8(52), 153-163, 1969.*

Mätzler, C., and U. Wegmüller, Dielectric properties of fresh-water ice at microwave frequencies, *J.Phys.D:Appl.Phys.,* 20, 1623-1630, 1987.

Maykut, G. A., Energy exchange over young sea ice in the central Arctic, *J.Geophys. Res.,83*(C7), **3646-3658, 1978.**

Maykut, G. A., Large-scale heat exchange and ice production in the central Arctic, *J. Geophys. Res., 87(C10), 7971-7984, 1982.*

Meese, D. A., *The Chemical and Structural Properties of Sea Ice in the Southern Beaufort Sea, CRREL Rep. 89-25,* U. S. Army Corps of Engineers, Cold Regions Research and Engineering Laboratory, Hanover, New Hampshire, 1989.

Nakawo, M,, and N. K. Sinha, Growth rate and salinity profile of first-year sea ice in the high arctic, *J. Glaciol., 27(96), 315-330, 1981.*

Nghiem, S. V., M. Borgeaud, J. A. Kong, and R. T. Shin, Polarimetric remote sensing of geophysical media with layer random medium model, *Progress in Electromagnetics Research, vol. 3:Polarimetric Remote* Sensing, chap. 1, ed. by J. A. Kong, pp. 1-73, Elsevier, New York, 1990.

Nghiem, S. V., S. H. Yueh, R. Kwok, and F. K. Li, Symmetry properties in polarimetric remote sensing, *Radio Sci.,27*(5), *693-711, 1992.*

Nghiem, S. V., T. Le Toan, J. A. Kong, H. C. Han, and M. Borgeaud, Layer model with random spheroidal scatterers for remet e sensing of veget at ion canopy, *J. Elec tromagn. Waves Appl.*, *7(1)*, *49-76*, 1993a,

Nghiem, S. V., R. Kwok, J, A. Kong, and R. T. Shin, A model with ellipsoidal scatterers for polarimetric remote sensing of anisotropic layered media, *Radio Sci.*, 28(5), 687-703, 1993b.

Nghiem, S, V., S. H. Yueh, R. Kwok, and D. T. Nguyen, Polarimetric remote sensing of geophysical medium structures, *Radio Sci.*, *28*(6), 1111-1130, 1993c.

Papoulis, A., *Probability, Random Variables, and Stochastic Processes,* McGraw Hill, *New* York, 1984.

Petrenko, V. F., *Structure of Ordinary Ice* I_h, *CRREL Rep. 93-25*, U. S. Army Corps of Engineers, Cold Regions Research and Engineering Laboratory, Hanover, New Hampshire, 1993.

Richter-Menge, J. A., and D, K. Perovich, Surface characteristics of lead ice, *Supplement to EOS, Transactions, American Geophysical Union, 73(43), 290,* Oct. 1992.

Rignot, E., and M. R. Drinkwater, Winter sea ice mapping from multi-parameter synthetic aperture radar data, *J. Glaciol.*, in press, 1994,

Sihvola, A. H., and J. A. Kong, Effective permittivity of dielectric mixtures, *IEEE Trans. Geosci. Remote Sens., 26(4), 420-429, 1988.*

Stogryn, A., and G. J. Desargant, The dielectric properties of brine in sea ice at microwave frequencies, *IEEE Trans. on Antennas and Propagat., AP-33(5), 523-532,* May 1985.

Thorndike, A. S., D. A. Rothrock, G. A. Maykut, and R, Colony, The thickness distribution of sea ice, *J. Geophys. Res.,* 80(33), 4501-4513, Nov. 1975.

Tiuri, M. E., A. H. Sihvola, E. G. Nyfors, and M. T. Hallikainen, The complex dielectric constant of snow at microwave frequencies, *IEEE Journal of Ocean Engineering, OE-9(5), 377-382,* December 1984.

Tjuatja, S., A. K. Fung, and J. Bredow, A scattering model for snow-covered sea ice,

IEEE Trans. Geosci. Remote Sens., *30*(4), *804-810, 1992,*

Tsang, L,, and J. A. Kong, Scattering of electromagnetic waves from random media with strong permittivity fluctuations, *Radio Sci.*, *16*(3), *303-320,* May-June 1981.

Tsang, L., J. A. Kong, and R. T. Shin, *Theory of Microwave Remote Sensing*, John Wiley, New-York, 1985,

Weeks, W, F., and A, J. Gow, Preferred crystal orientations in the fast ice along the margins of the Arctic Ocean, *J. Geophys. Res.*, 8S'(C1O), 5105-5121, 1978.

Weeks, W. F,, and S. F. Ackley, *The Growth, Structure, and Properties of Sea Ice, Monogr. Ser.*, Vol. 82-1, U, S. Army Corps of Engineers, Cold Regions Research and Engineering Laboratory, Hanover, N. H., 1982,

Wen, T., W. J. Felton, J. C. Luby, W. L. J. Fox, and K. L. Kientz, "Environmental Measurements in the Beaufort Sea, Spring 1988," *Technical Report,* APL-UW TR 8822, Applied Physics Laboratory, University of Washington, Seattle, Washington, 1989.

Wettlaufer, J. S., Heat flux at the ice-ocean interface, *J. Geophys. Res.*, *96*(C4), 7215-7236, 1991.

Wright, J. W,, A new model for sea clutter, *IEEE Trans. Antennas Propagat.*, *AP-16*, *217-223, 1968.*

Yueh, H. A,, R, T. Shin, and J. A. Kong, Scattering from randomly oriented scatterers with strong permittivity fluctuations, *J. Electromagn. Waves Appl.*, *4(10), 983-1004, 1990,*
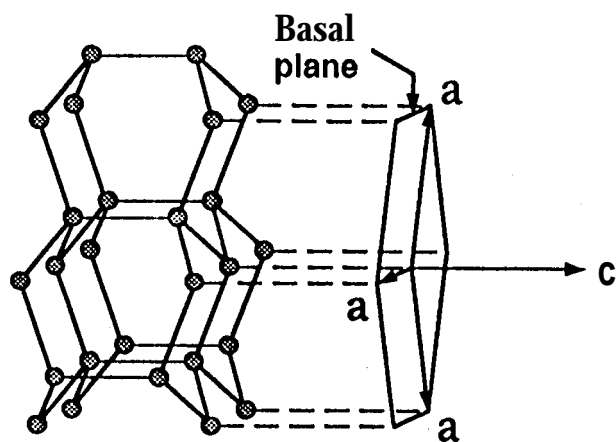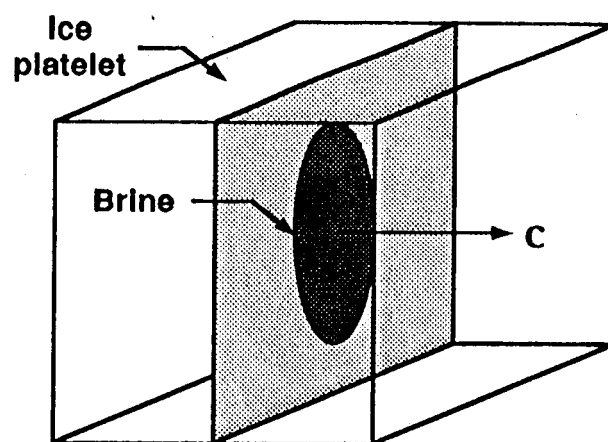
LIST OF FIGURES
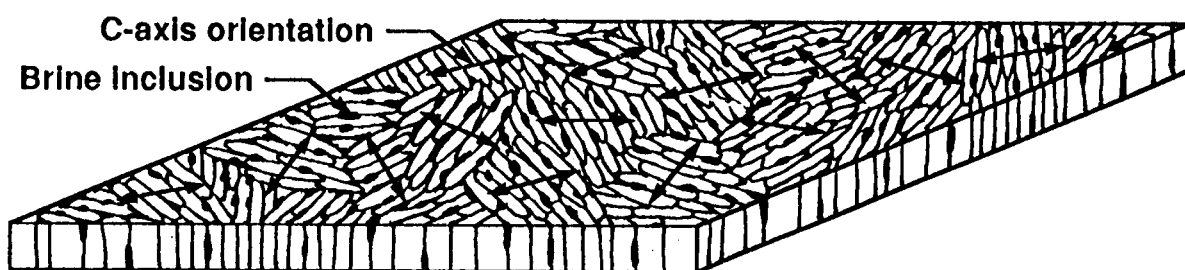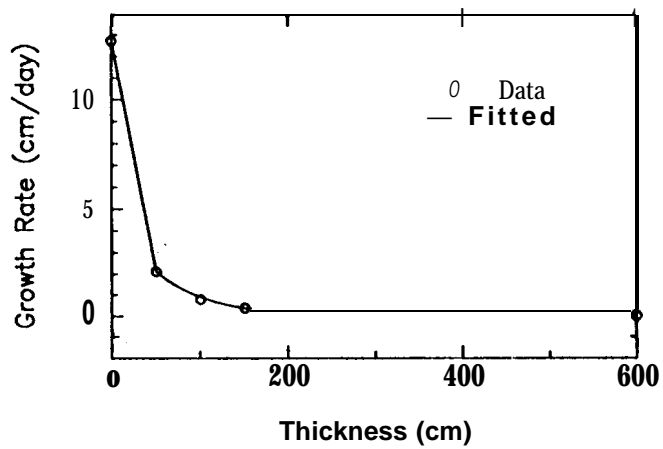
Figure 1

Figure 2

Figure 3

(a) Growth Rate of Sea Ice on March 11
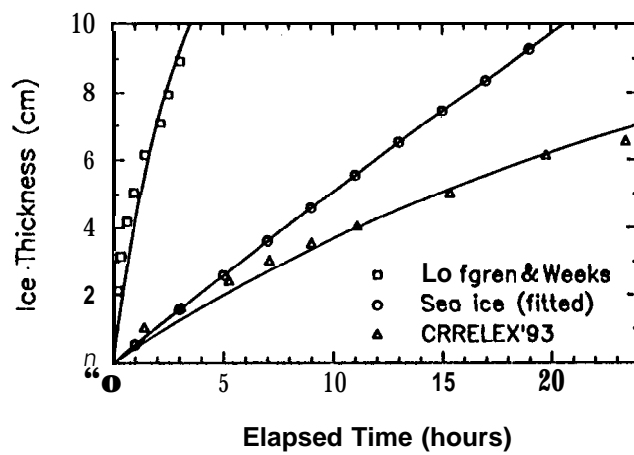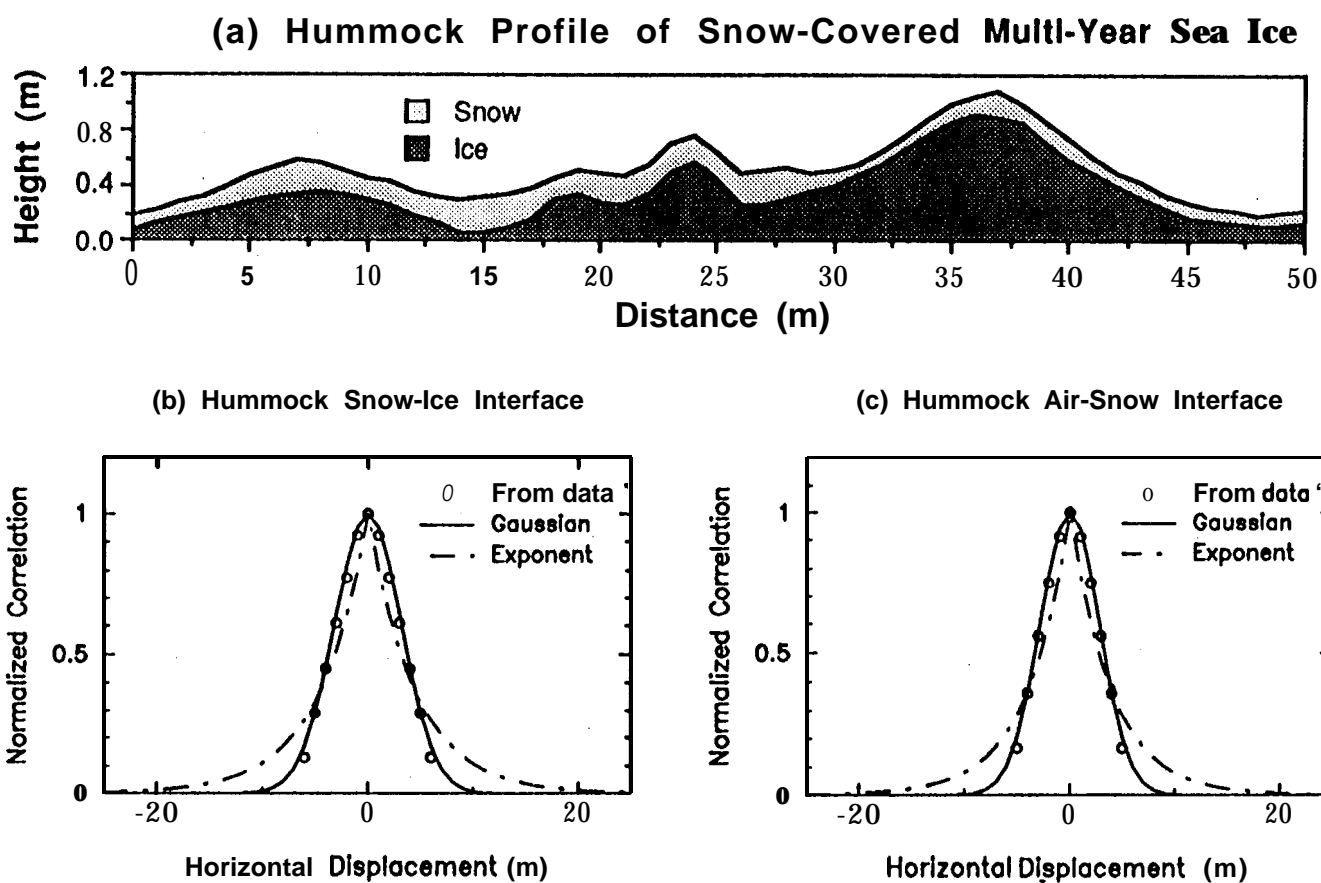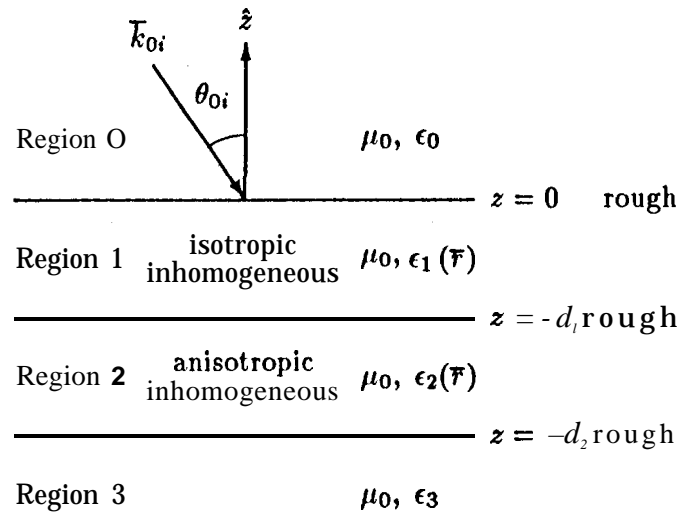

(b) Growth of New Ice (O-1 O cm)

FIGURE 4

(a) Hummock Profile of Snow-Covered Multi-Year Sea Ice

Height (m)

1.2
0.8
0.4
0.0

☐ Snow
■ Ice

0   5   10   15   20   25   30   35   40   45   50

Distance (m)

(b) Hummock Snow-Ice Interface

Normalized Correlation

1

0.5

0

-20   0   20

o   From data
——   Gaussian
—·— Exponent

Horizontal Displacement (m)

(c) Hummock Air-Snow Interface

Normalized Correlation

1

0.5

0

-20   0   20

o   From data "
——   Gaussian
—·— Exponent

Horizontal Displacement (m)

FIGURE 5

Figure 6

Region 0 $\overline{B}_0$ $\overline{A}_0 = \overline{\overline{R}}_0 \cdot \overline{B}_0$

$z = 0$

Region 1 $\overline{A}_1$ $\overline{B}_1 = \overline{\overline{D}}_1 \cdot \overline{B}_0$

$z = -d_1$

Region 2 $\overline{B}_2$ $\overline{A}_2 = \overline{\overline{U}}_2 \cdot \overline{B}_0$

$z = -d,$

Region 3 $\overline{B}_3 = \overline{\overline{T}}_3 \cdot \overline{B}_0$

Figure 7

Figure 8